Available online at www.sciencedirect.com

SciVerse ScienceDirect

Energy Procedia 37 (2013) 5692 – 5701

Energy Procedia

GHGT-11

Development of reacted channel during flow of CO_2–rich water along a cement fracture

Nicolas J. Huerta*[,a,c], Quinn C. Wenning[a], Marc A. Hesse[a], Steven L. Bryant[b], Christina L. Lopano[c], Brian R. Strazisar[c]

[a]*The University of Texas at Austin, Jackson School of Geosciences, 1 University Station, Austin, TX 78712, USA*
[b]*The University of Texas at Austin, Petroleum and Geosystems Engineering, 1 University Station, Austin, TX 78712, USA*
[c]*US Dept. of Energy, National Energy Technology Laboratory, 626 Cochrans Mill, Pittsburgh, PA 15236, USA*

Abstract

Lab scale experiments were performed to characterize how coupling between reaction and flow affect time-dependent flux of CO_2-rich water along leaky wells. The core flow system applies confining stress to a cement core with a single tensile fracture while CO_2-rich water is injected at constant rate and elevated pore pressure. Results show no significant variation in pressure differential, despite the development of a texturally distinct calcium depleted channel along the fracture surfaces which is bounded by thin rims of precipitation. Silicon rich material remains in the channel and prevents wormhole development and large increases in aperture. Implications for time-dependent CO_2 leakage are that even with high fluid flux, the leak does not get appreciably worse.

Selection and/or peer-review under responsibility of GHGT

Keywords: wellbore; zonal isolation; cement; fracture; reactive transport; dissolution; precipitation

* Corresponding author. Tel.: +1-512-557-7652;

E-mail address: njhuerta@utexas.edu (N. Huerta).

1876-6102
Selection and/or peer-review under responsibility of GHGT
doi:10.1016/j.egypro.2013.06.491

1. Introduction

Long-term risk assessment of any CO_2 sequestration project must assign not only a likelihood of leaking wells, but also an estimate of the magnitude of the leak rate and how it changes over time. While leakage of bulk phase CO_2 is an obvious concern, the migration of CO_2-rich brine may be of greater importance during injection. The nature of multiphase flow guarantees that the plume of CO_2-rich brine will be as large as the CO_2 plume [1], and the widespread increase in fluid pressure during large-scale injection will provide sufficient driving force to displace that brine along leaky wells. Possible consequences include contamination of shallow water resources and exacerbating the leakage pathway. The latter is possible when chemical reaction and flow are coupled.

Leakage paths along wells are subject to geomechanical stresses, so one mode of coupling arises when chemical reactions alter the mechanical strength of the materials [2,3]. The stress-strain response can alter the aperture of the leakage path. Here we examine the consequences when volumes of minerals along the flow path are precipitated or dissolved as reactive fluid migrates. Experiments are essential for characterizing coupled phenomena of reactive transport along a leak path. Injection of reactive fluid through rocks [4] and along fracture surfaces [5] may lead to self-enhancing flow paths (wormholes, channels) for a certain range of Damkohler numbers (ratio of characteristic flow speed to characteristic reaction speed) [6].

In previous work with an analog geochemical system we found behavior that tended toward self-limiting in a leakage path representative of a likely field situation (a rough-walled fracture within cement) using dilute hydrochloric acid to represent CO_2-saturated brine [7]. In this work we show that leakage of CO_2-rich water (composition typical of storage conditions) through fractured cement exhibits similar behavior as the analog system. In the hydrodynamic conditions likely to apply in sequestration, this behavior should tend toward self-limiting or self-sealing leaks of CO_2-rich brine.

2. Methods

2.1.1. Sample preparation

We represent a leakage path as a rough-walled fracture along the length of cylindrical cement sample. Samples were created by the same method described in Huerta et. al [7]. The process of creating each fractured sample does not produce fractures of uniform hydraulic aperture and leads to variation in sample length. However, samples were chosen with these two properties as similar as feasible.

2.1.2. Flow equipment

We used a core flow unit purchased from Coretest Systems Inc. (CFS-839Z). This unit can perform single or multiphase flow of liquid and CO_2 in various phases through a core held in a uniaxial Hassler cell. The system can operate at reservoir conditions of pore pressure and temperature.

To generate CO_2-rich water, we modify the unit to promote dissolution of CO_2 with a liquid phase by mixing between two accumulators. We first calculate the theoretical maximum dissolved CO_2 for the experimental conditions using an equation of state [8]. The series of experiments reported here is intended to maximize carbonic acid concentration and hence the potential for mineral precipitation (the result of carbonate anions mixing with divalent cations released from cement matrix). Thus we used deionized water and a temperature of 21 °C to obtain a dissolved CO_2 concentration of 6.3 wt.%.

The liquid accumulator was then filled with deionized water and the system was brought up to pressure using that liquid. This approach also served to pre-flush the core with a reactive fluid (pH 7, unsaturated with respect to cement matrix minerals) to simulate leakage of many fracture volumes (e.g. 0.07 mL = 1 fracture volume for NA7-11) of fluid along the wellbore. Typically a few hundred mL of water were

used. The equivalent fracture geometry was determined from the flow rate and pressure drop measurements, modeling the fracture as a slit between parallel plates [9]. The equation is:

$$Q = \frac{B_{Hyd}^3 W}{12} \frac{P_{up} - P_{down}}{\mu L}$$

With the following definitions: Volumetric flow rate (Q), hydraulic aperture (B_{Hyd}), fracture width (W), upstream pressure (P_{up}), downstream pressure (P_{down}), fluid viscosity (μ), and fracture length (L).

2.2. Analysis equipment / methods

Effluent element analysis was performed using a Perkin Elmer model Optima 3000 XL coupled plasma atomic emission spectrometer. Fracture surface images were collected using a digital camera. Scanning Electron Microscopy (SEM) was performed with a Philips/FEI XL3. Environmental SEM was used on the uncoated and unpolished fracture surfaces. Conditions were 20.0kV accelerating voltage, 0.1 Torr chamber pressure, and a working distance of 10.7 mm for Secondary Electron (SE) imaging, Back Scattered Electron (BSE) imaging, and qualitative Energy-Dispersive X-ray Spectroscopy (EDS). Micro X-ray Diffraction (μXRD) was performed with a Rigaku R-Axis micro diffractometer equipped with an UltraX18 Cu rotating anode X-ray source and Rapid II 180-degree curved imaging plate detector. X-rays were collimated to a 100 micron spot size. Phase identification was performed using the Rigaku PDXL software equipped with the ICDD PD4 database.

3. Results

3.1. Experiment summary

Table 1: Summary of conditions and results for each experiment

Sample name	NA7-11	NA9-3	QB4-3	QB6
Dimensions (Width / Length), cm	2.54 / 6.25	2.54 / 5.37	2.54 / 7.24	2.54 / 6.17
Flow rate, mL/min	1.0	0.5	0.25	3.0
Time, min	477	2,827	3,035	474
Volume injected, mL	477	1,414	759	1,300
Total CO_2 injected, mmol	691	2,008	1,092	1,870
Initial pressure differential, psi	0.90	0.35	0.20	7.50
Final pressure differential, psi	0.70	0.30	0.20	5.00
Initial hydraulic aperture, μm	43	44	47	30
Final hydraulic aperture, μm	47	47	47	38

Results from four constant flow rate experiments are summarized in Table 1. Confining pressure was 1,500 to 1,600 psi for all experiments and pore pressure was between 1,000 to 1,100 psi. The key

independent variables for each experiment were the flow rate, which ranged from 0.25 to 3.0 mL/min, and the duration of the experiment. These two independent parameters affect total fluid injected.

3.2. Pressure differential and effluent cation concentration history

As an example, the pressure differential and effluent history for sample NA7-11 are plotted in Figure 1 as a function of cumulative mmol of CO_2 injected. Pressure plot (Figure 1 – Top left) shows an early decline until 200 mmol of CO_2 injected followed by a plateau. The pressure differential is rather small, with hydraulic aperture evolving from 43 μm (dP = 0.9 psi) through a maximum of 48 μm (dP = 0.65 psi) to 47 μm (dP = 0.7 psi). NA9-3 and QB4-3 pressure trace remain flat and corresponding aperture show little change (Table 1). Sample QB6 has a larger change in pressure differential at the end of the experiment but is within noise for most of the experiment and could be related to injection of the free phase CO_2 cap in the accumulator. In all experiments there was no significant and sustained decrease in pressure differential as one would expect if the size of the pathway had increased. However, there was also no significant pressure spike that might imply pathway sealing.

Effluent was collected at various time increments, and sample NA7-11's results are shown in Figure 1. Effluent calcium is the dominant species and concentration is shown in Figure 1 (Top right). Concentration spikes to above 500 mg/L early, then drops to just above 300 mg/L, rises back up to a maximum at 550 mg/L and then begins to decrease at a roughly constant rate to 250 mg/L when flow was terminated. The general pattern of an early spike followed by a gradual drop to an intermediate value is observed in all experiments. Time to reach the initial spike shows no correlation with flow rate. However, slower flow tends to yield a larger effluent concentration spike. Calcium concentrations are typically an order of magnitude larger than other relevant species. Figure 1 (Bottom right) shows effluent silicon concentration. In all experiments effluent silicon concentration begins with an early spike and decays to some base concentration, usually below 15 mg/L, before 500 mmol of CO_2 injected. The spike of silicon is correlated to the flow rate, with the slowest flow rate having the largest spike and the fastest flow having the smallest spike (QB4-3 at 100 mg/L and QB6 at 25 mg/L respectively). Other species (not shown) following this trend are magnesium, and sulfur. Effluent aluminium and iron concentrations in all experiments are low (often below detection limits), considering their concentration in cement. As an example, iron concentration for NA7-11 is plotted in Figure 1 (Bottom left).

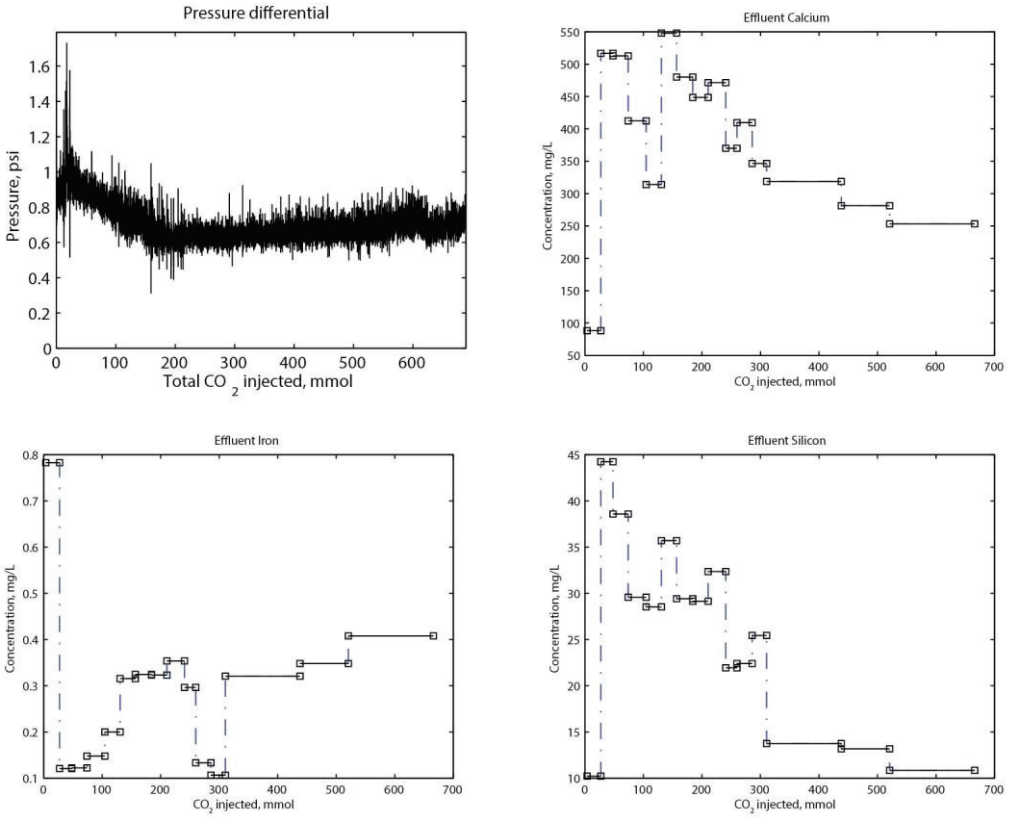

Figure 1 – **Sample NA7-11**. All values are plotted as a function of dissolved CO_2 injected. (Top left) Pressure differential. (Top right) Effluent calcium concentration. (Bottom left) Effluent iron concentration. (Bottom right) Effluent silicon concentration.

3.3. Fracture surface analysis

Figure 2 (Left) shows an image of the fracture surface after experiment completion. A distinct reacted channel has developed on the surface that is larger at the inlet and decreases toward the outlet. Narrow bands of white mineral precipitate are concentrated along some of the channel edges, especially along the left side of the channel in the picture. Other portions of the channel edge are typically broad and light gray, for example the right channel boundary near the outlet. In the other three experiments the reacted channel is much broader, often taking up nearly the entire width. In two of the samples there are significant choke points (NA9-3 and QB4-3). In the experiment with largest flow rate there are several distinct ‘islands’ that are perpendicular to the bulk flow direction that are bounded by thin bands of precipitation.

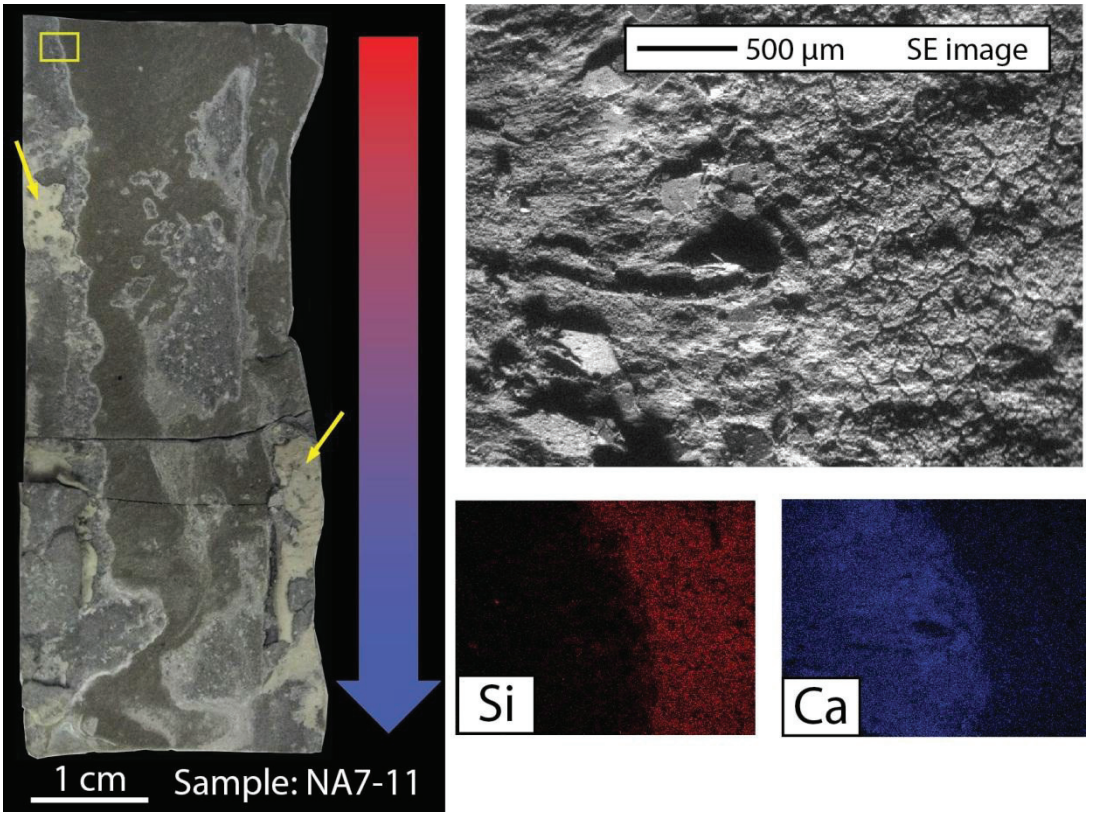

Figure 2 – (Left) Image of sample fracture surface after injection of CO_2-saturated water. Note that the rough shape on the right side of the core was due to sample breaking after experiment. In this experiment a distinct channel has formed and is wider at the inlet (top) and narrows toward the outlet (bottom). White caulk is identified by the yellow arrows. The yellow box is the location picked for SEM/EDS analysis. (Top right) SE image of the yellow box area. The textural roughness of the sample is evident. (Bottom images) EDS element maps of the yellow area. (Bottom right) Calcium is relatively higher on the left side, which is out of the reacted channel. (Bottom left) Due to calcium leaching, silicon becomes relatively enhanced in the channel.

3.4. Fracture surface and SEM / EDS analysis

We performed SEM/EDS on sample NA7-11 to characterize changes on the fracture surface with respect to morphology and element concentration. The yellow box in Figure 2 (Left) highlights the region studied. Figure 2 (Top right) shows a SE image of the region. The difference in local topography (cracked area on the right, combination of fine grained material and distinct euhedral crystals on the left) corresponds respectively to the reacted flow channel and unreacted surface on either side of the white precipitate evident in the photograph. The BSE image in Figure 3 (Top left) more distinctly shows region morphology. The right hand side has distinct polygonal cracking and on the left side there is a combination of lighter colored material that are the euhedral crystals and darker material that is the unreacted cement. Figure 2 also shows element maps for calcium (Bottom right) and silicon (Bottom left). Calcium is inferred to be leached from the reacted channel (right side), which causes a relative enrichment of silicon.

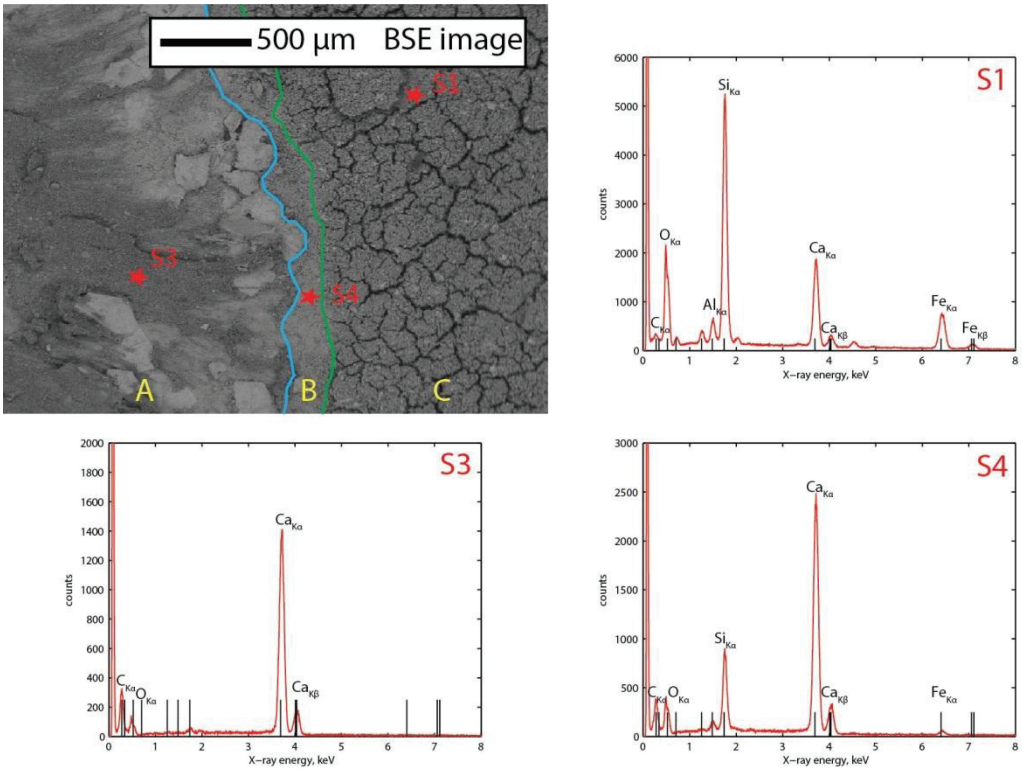

Figure 3 – (Top left) BSE image of study area in NA7-11 with distinct zones identified. (S1) Spot analysis of reacted zone. Note silicon K_α peak is higher than the calcium K_α which is a qualitative indication of concentration. (S3) Spot analysis of unreacted zone. The relative counts of the K_α peaks indicate calcium is dominant. (S4) Spot analysis of transition zone. The ratio between silicon and calcium signal is in between the two end member zones.

Based on texture and spot maps we can identify three distinct zones Figure 3 (Top left).

Zone A – Unreacted cement zone

This zone is characterized by fine grain unreacted cement and euhedral crystals. The crystals are probably portlandite precipitated after the core was fractured, assembled, and then placed back in water before being used for experiments. There is a possibility that carbonation from atmospheric CO_2 has altered the portlandite to calcite. EDS spot analysis shows this zone is enriched in calcium relative to other key elements (Figure 3 - S3).

Zone B – Transition zone

This zone includes both the narrow white interface and the broader light grey boundary between flow channel and unreacted cement zone seen in plain light images (Figure 2).This zone is characterized by distinct euhedral rhombs that precipitate in and around a finer matrix of material. These euhedral crystals are much smaller than those present in the unreacted cement. In the zones where the plain light showed a distinct narrow white band, the euhedral crystals often align along the boundary. In the broader light grey zone, the crystal rhombs are present but often have a sheared or eroded look. EDS of this zone shows that silicon is becoming relatively more enriched but calcium still dominates (Figure 3 - S4).

Zone C – Reacted zone

In the reacted zone the solid surface has large polygonal cracks. Zooming in on this zone we see no distinct crystals and the material is fine grained. EDS of this zone shows calcium depletion and silicon and iron are relatively enriched (Figure 3 - S1).

3.5. μXRD analysis

Sample QB4-3 was selected for mineral identification in the intermediate zone because of the distinct precipitated zone pinching the reacted channel (Figure 4 Left). Figure 4 (Top right) shows an image of the specific area analyzed and the plot of identified minerals is also shown (Bottom right). Calcite, portlandite, and some vaterite were identified.

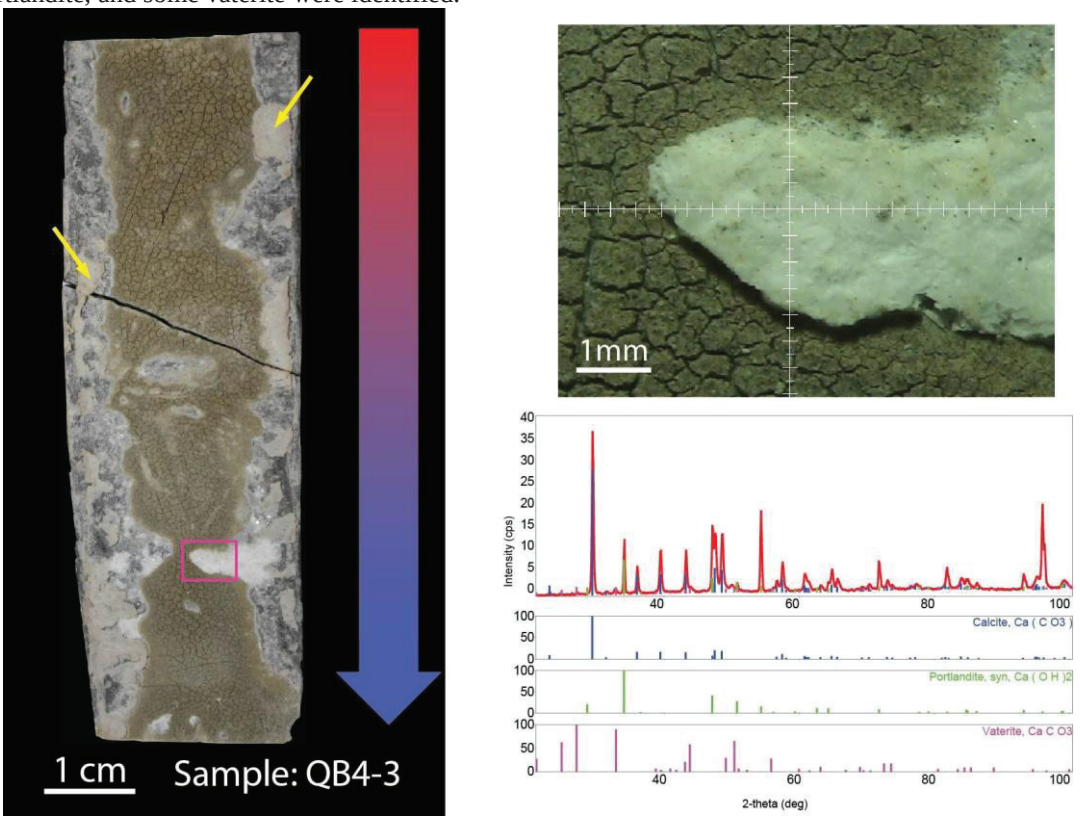

Figure 4 – (Left) Image of fracture surface. Yellow arrows point to caulk on sample. Magenta box identifies zone where precipitate pinches flow channel. (Top right) Image of precipitate analyzed in sample QB4-3. (Bottom right) Plot of intensity (counts) versus 2-theta angle diffraction pattern with the corresponding mineral identification of calcite, portlandite, and vaterite in the intermediate zone.

4. Discussion

In all experiments, CO_2-rich waters injected into the cement core caused a distinct reacted (Zone C) channel that is bounded by secondary minerals (Zone B) to develop. This channel development is similar to observations in an analog geochemical system presented in Huerta et al. [7]. In that work they also found the channel depleted in calcium relative to silicon. They also identified calcite precipitating in the

transition zone. We propose that the same mechanism is involved in this system. As the CO_2-rich water (and the source of carbonic acid) is injected into the core, local pH drops and portlandite and calcium silicate hydrate (C-S-H) become soluble and calcium is liberated. While portlandite undergoes total dissolution, C-S-H leaves behind an amorphous silica rich phase that prevents significant opening of the fracture and wormhole development. Effluent data is consistent with this observation: substantial calcium is extracted from the core but silicon quickly drops to a low concentration in the effluent. Due to the heterogeneous nature of the fracture surface, slow flow regions (with small local aperture and rich in hydroxide ions), interface with waters rich in calcium and carbonate. The pH rises and calcite then becomes insoluble and begins to precipitate in this transition zone.

Though a distinct reacted channel formed in each experiment, none showed a distinct change in pressure differential. This is despite many fracture volumes injected. The absence of a pressure differential decrease is because total dissolution of the cement material does not occur. The remaining silicon rich phase prevents significant pathway opening and wormhole development that is commonly observed in in carbonate rocks. Rapid drop off of effluent silicon concentration also indicates that material in the reacted channel remains to prevent pathway enhancement. It is expected that as more fluid is injected, reaction with the cement would become limited by diffusion into the cement core and therefore leak path conductivity would not increase significantly.

Unlike previous work with an analog geochemical system [7] no significant increase in pressure differential was observed here. This might be explained by several observations. First is the observation of CO_2 bubble exsolution in the effluent stream early in the experiment. This is evidence for kinetically limited reactions in the core. The fluid either cannot speciate rapidly enough to generate more carbonic acid or the dissolution/precipitation rates are significantly slower than residence time in the core. There is also an inverse correlation in these four experiments between flow rate (and residence time) and effluent calcium concentration. In the analog system where hydrochloric acid was used, the aggressive nature of the strong acid allowed rapid reaction, which resulted in effluent pH concentration remaining high for a significant part of the experimental duration. The net result is that there is much more calcium available to precipitate and form more barriers to flow early on.

The in-situ system will have a significantly longer leakage path, slower overall fluid flux, and be driven by pressure gradient, rather than by an imposed flow rate. All three factors are likely to amplify the self-sealing tendencies suggested in our laboratory-scale experiments. With a longer leakage pathway and slower fluid flux, fluid residence time increases. More residence time increases diffusion of calcium from cement phases, ensures more acid is reacted, and allows for more interface time between high pH waters and the calcium and carbonate rich fluids. All of this allows greater carbonate precipitation. If flow is driven by a fixed pressure drop, any reduction in the flow caused by precipitation increases residence time further, and thus the coupled system tends toward self-sealing behavior.

5. Conclusions

Our experiments have shown that CO_2-rich water injected into neat class H cement produces reaction patterns similar to those in diffusion dominated batch reaction experiments and also in analog fracture flow experiments using a more aggressive acid. Dissolution of calcium-rich cement phases and precipitation of calcium-rich minerals cause the development of flow channels within the fracture. Reaction kinetics are slower than for aggressive acid and channels consequently tended to be broader. Thus, pressure differentials did not show any significant precipitate-driven spike. The presence of amorphous silicate material left in the reacted channel after calcium leaching mitigates any self-reinforcing tendency in channel formation. These results are important for the forecasting of possible bounds on leakage risk, as the likelihood of self-enhancing leaks of CO_2-saturated brine along wellbores seems small based on our results.

Acknowledgements

This work was supported by the National Risk Assessment Program of the U.S. DOE National Energy Technology Laboratory and from sponsors of the Geological CO_2 Storage Industrial Affiliates Program at the Center for Petroleum and Geosystems Engineering at UT-Austin.

References

[1] Kumar A, Noh M, Pope GA, Seperhrnoori K, Bryant S, Lake LW. Reservoir simulation of CO_2 storage in deep saline aquifers. Soc Pet Eng J 2005; 10:336-348.

[2] Huerta NJ, Bryant SL, Strazisar BR, Kutchko BG, Conrad LC. The influence of confining stress and chemical alteration on conductive pathways within wellbore cement. Energy Procedia 2009; 1:3571-3578.

[3] Huerta NJ, Bryant SL, Strazisar BR, Hesse M. Dynamic alteration along a fractured cement/cement interface: Implications for long term leakage risk along a well with an annulus defect. Energy Procedia 2011; 4:5398-5405.

[4] Wang Y, Hill AD, Schechter RS. The optimum injection rate for matrix acidizing of carbonate formations. SPE 1993; SPE 26578.

[5] Hung KM, Hill AD, Sepehrnoori K. A mechanistic model of wormhole growth in carbonate matrix aciding and acid fracturing. J Petro Tech 1989; SPE 16886.

[6] Szymczak P, Ladd JC. Wormhole formation in dissolving fractures. J Geophys Res 2009; 114:1-22.

[7] Huerta NJ, Hesse MA, Bryant SL, Strazisar BR, Lopano CL. Experimental evidence for self-limiting reactive flow through a fractured cement core: Implications for time-dependent wellbore leakage. Environ Sci Technol 2012. In press.

[8] Duan Z, Sun R. An improved model calculating CO_2 solubility in pure water and aqueous NaCl solutions from 273 to 533 K and from 0 to 2000 bar. Chem Geol 2003; 193:257-271.

[9] Witherspoon PA, Wang JSY, Iwai K, Gale JE. Validity of cubic law for fluid flow in a deformable rock fracture. Water Resour Res 1980; 16:1016-1024.

[10] Kutchko BG, Strazisar BR, Dzombak DA, Lowry GV, Thaulow N. Degradation of well cement by CO_2 under geologic sequestration conditions. Environ Sci Technol 2007; 41:4787-4792.